J Therm Spray Tech
https://doi.org/10.1007/s11666-024-01884-3

ORIGINAL RESEARCH ARTICLE

Reusing 316L Stainless Steel Feedstock Powder for Cold Spray Deposition

Edwin Rúa Ramírez[1,2] · Alessio Silvello[1] · Edwin Torres Diaz[1,2] · Rodolpho F. Vaz[1,3] · Irene Garcia Cano[1]

Submitted: 15 July 2024 / in revised form: 29 October 2024 / Accepted: 7 November 2024

Abstract Cold spray (CS) is a solid-state deposition of coatings, or an additive manufacturing (CSAM) process employed to make parts maintaining the feedstock powders properties in the deposited material. One of the cons for industrial use of CS or CSAM is their higher costs compared to the traditional coating or manufacturing processes. Reducing the feedstock powder consumption by maximizing the deposition efficiency has been the focus of many works. However, depending on the part geometry (e.g., a plate with holes), and CSAM strategy with low deposition efficiency, a considerable mass of powder can pass through the substrate, failing to bond, and becoming a process waste. This work evaluates CS 316L stainless steel coatings, recovering the unbonded particles and reusing them in a later deposition, thus making coatings with reused powders. The original and recovered powders were characterized in terms of particle shape and size distribution, phase composition, microhardness, and other properties to evaluate the evolution of the particles' properties due to the recovery process. Besides the powders, the CS coatings obtained with original and recovered powders were evaluated through cross-section image analysis, where porosity, deposition efficiency, and microhardness were observed. The results indicate that the powders' physical properties undergo variations over multiple deposition cycles without significantly affecting the quality of the CS coatings, with porosity below 1.5% and microhardness around 350 $HV_{0.3}$ in most cases. Recovering and reusing powder for CS promotes environmental sustainability and generates significant economic benefits. This study contributes to making CS more economically viable from a life cycle cost assessment perspective.

✉ Alessio Silvello
asilvello@cptub.eu

[1] Thermal Spray Center (CPT), Universitat de Barcelona, Carrer de Martí i Franquès 1, 08028 Barcelona, Spain

[2] Mechanical Engineering, Research USTA (IMECI-USTA), Santo Tomás University, Tunja, Colombia

[3] Center for Thermal Spray Research (CTSR), Stony Brook University, Room 130 Heavy Engineering Bldg, Stony Brook, NY 11794, USA

Graphical abstract

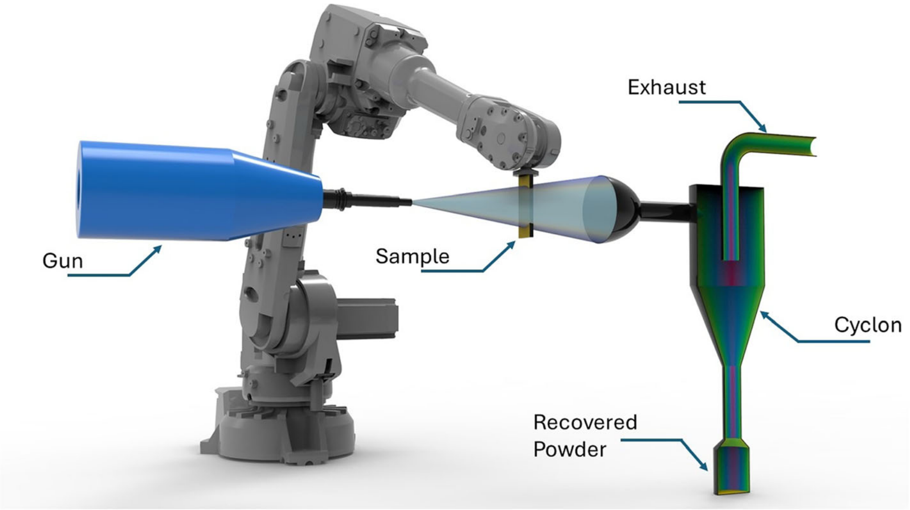

Keywords cold spray · 316L stainless steel · coatings · reuse · sustainability · circular economy

Introduction

Cold spray (CS) is an advanced solid-state deposition technique for coating and building three-dimensional structures layer-by-layer, called, in this case, cold spray additive manufacturing (CSAM). CS or CSAM operates by spraying particles dragged by an accelerated gas, reaching supersonic speed, at much lower temperatures than thermal spraying or other AM techniques. It prevents the melting or degradation of the substrate and the feedstock powder (e.g., phase transformation, oxidation, and thermal residual stresses), which is attractive for complex alloys, such as high entropy alloys (HEAs), Al, Ti, and other thermal- or oxygen-sensitive materials. The CS-ed particles' bonding mechanism is the severe plastic deformation of the materials upon their impact onto the substrate below the material recrystallization point, improving the CS-ed material's properties by cold working (Ref 1-3). For CSAM, different strategies have been developed to make complex geometries, based on controlling the gun/substrate angle and path; however, for CS coatings the best option is using the traditional thermal spraying strategy, guaranteeing the gun/substrate normal angle by following a zig-zag-like or raster path on the substrate surface (Ref 4).

Among the materials deposited by CS, 316L stainless steel, simply named 316L in this work, has been widely used in different industrial sectors, such as biomedical, pharmaceutical, oil and gas, and food industries, among others. CS has emerged as a technique for 316L deposits due to its characteristic of maintaining the feedstock properties after deposition, avoiding grain growth, δ ferrite or σ phase formation, sensitization, and other deleterious effects seen in melting-based 316L processing [e.g., arc-welding (Ref 5) or laser cladding (Ref 6)].

Regarding the feedstock material for CS, it must be a powder, which can be obtained by different methods (e.g., gas-, plasma-, or water-atomizing, oxide reduction, mechanical alloying, melting spinning, sintered and crushed, and agglomeration, among others). It results in diverse powder characteristics: irregular or spherical shape, larger or smaller size, and dense or porous particles, among others. For CS, the feedstock powder affects the particle bonding and the coating properties because the particle size alters the velocity window of deposition, which is a range of velocity values between a minimum velocity to promote the particle bonding, v_{critical} or v_{cr}, and a velocity in which the particles erode the substrate instead to bond onto it, v_{erosion}, for the particle bonding by adiabatic shear instability (ASI) (Ref 2), as well as jetting, mechanical interlocking, and other mechanisms (Ref 3, 7). Particle shape (irregular or spherical) interferes on the particle velocity because the drag coefficient varies with the spheroidicity, and irregular particles have higher coefficient than the spherical ones (Ref 8). Besides that, small particles increases the v_{cr} and large particle has higher inertia to reach the v_{cr}, resulting in an ideal particle size distribution of $-60+10$ µm (Ref 3).

Spherical powders have been used for CS deposition as for other manufacturing processes, such as welding or other additive manufacturing (AM) processes; however, spherical powders are much more costly than irregular ones. To evaluate the possibility of using a less costly powder for CSAM, Vaz et al. (9) compared 316L deposits made with both powders and concluded that both had similar microstructures, microhardness, corrosion performance, and wear resistance, resulting in a reduction in the CSAM parts building by depositing an irregular powder; Bhattiprolu et al. (10) also showed that a low-cost hydride–dehydride and a costly gas-atomized Ti6Al4V resulted in close adhesion strength, porosity, and microhardness.

As the ASI mechanism depends on the particle deformation, hard particles or hard phases in the powder have to be avoided in order to guarantee the material plasticity upon impact on the substrate (Ref 12). Regarding the powder purity, the degree of oxidation reduces the Cu deposition efficiency (DE) and increases drastically the v_{cr}. Li et al. (13) presented that when the oxide content of the Cu powder was increased from 0.02 to 0.38 wt.%, the v_{cr} increased from 300 to 610 mm s^{-1}. However, the same deleterious effect is not reported in the literature for 316L.

Since the material consumption in CS depends on the materials, CS-ed area, CSAM-ed part size, DE, and others, the deposition costs are highly affected by the feedstock powder acquisition. Focusing on the recovery of the undeposited powders by CS and reusing supports the principles of environmental sustainability by promoting the reuse of resources and reducing the deposition costs through recycling waste material. This approach is beneficial to sustainability and can potentially improve the profitability of the CS coating technique. Thus, the integration of eco-efficient practices into CS processing is not only in line with today's environmental requirements but also supports the long-term viability of this coating technology.

Research and development related to recycling and reuse, and the search for alternatives are highly relevant to reap the benefits of thermal spraying techniques such as CS are relatively environmental friendly technologies (Ref 14), and there is scarce literature about reusing CS-ed unbonded particles. For the laser powder bed fusion (LPBF) AM technique, recycling powder altered the O content and phase composition, presenting the deleterious δ ferrite with γ austenite in 316L (Ref 15); for direct energy deposition (DED), recycling generated agglomerate particles and porous recovered 316L powder; however, it did not affect the deposit properties made with recycled and sieved powder (Ref 16). The present work evaluates the effect of recovering CS-ed unbonded 316L particles on the powder characteristics and properties, contributing to understanding the viability of reuse powder for CS. This evaluation is based on the power changes after CS. For CS, the apparatus for recovery of particles is more complex than for LPBF and DED, in which the powder does not flow at high velocity as it does in CS. It requires a special apparatus for collecting the CS-ed and unbonded particles, which was designed for the experiment presented in this work.

This work evaluates the 316L feedstock powder characteristics and properties evolution with the recovering, measuring, and discussing the particle size distribution, flowability, apparent density, shape, material phase composition, and microhardness. Besides the powders, CS-ed coatings were made with each powder condition: original, recovered once, and recovered twice. The coatings were characterized by their microstructure, porosity, microhardness, and DE. In addition, an economic analysis of the effect of recycling powder indicated the effectiveness in cost reduction for a CS deposition.

Materials and Methods

The experiments consisted of depositing 316L powder by CS using two different CS systems. During the CS deposition, the unbonded particles were recovered by a collector apparatus, and this recovered powder was sprayed again. Table 1 lists the samples names, systems, and feedstock powder characteristics. The properties of the powders and CS coatings were characterized in combination of spray condition each step. The apparatus for recovering the unbonded powder consisted of a cyclone (Fig. 1), and its design considered the CS gun size, nozzle geometry, and physical constraints in the spraying booth. The cyclone recovery efficiency (CRE) was measured by the ratio between the unbonded particle mass and the recovered mass, using (1), where CRE is expressed as %, $P_{\mathrm{recovered}}$ is the recovered powder mass in g, P_{sprayed} is the powder fed in g, and P_{coating} is the deposited coating mass in g. It is important to affirm that the CS system is cleaned at the end of the working day and the amount of residual powder is low enough to be neglected in P_{sprayed} measuring.

$$\mathrm{CRE} = \frac{P_{\mathrm{recovered}}}{P_{\mathrm{sprayed}} - P_{\mathrm{coating}}} \qquad \text{(Eq 1)}$$

Powders Characterization

The Daye 316L (Shijiazhuang, China) feedstock powders were characterized in the original and recovered conditions. The determination of particle size distribution was done by laser scattering (LS) technique using a Beckman Coulter LS 13 320 (Brea, CA, USA) equipment in dry mode, in accordance with the ASTM B822-02 standard. The images were obtained by scanning electron microscopy (SEM) using a Jeol 6510 (Tokyo, Japan) microscope. Phase analyses were performed by x-ray diffractometry (XRD) in a Malvern PANalytical X'Pert PRO MPD (Malvern, United Kingdom) h/h Bragg-Brentano, equipped with Malvern X'Pert HighScore Plus v.2.0.1 software. This technique used a Co Kα (λ = 1.7903 Å) with an operating power of 45 kV and 40 mA. The Scherrer equation (2) was used to measure the mean size of the ordered grains or crystallite. τ is the crystallite size, K is a shape factor

Table 1 CS-ed coatings samples description

Sample name	System	Powder characteristic
PCS100_0	PCS100	316L original
PCS100_1	PCS100	316L 1st recovery
PCS100_2	PCS100	316L 2nd recovery
PCS100_3	PCS100	75wt.% 316L 2nd recovery + 25wt.% 316L original
Kinetiks_0	Kinetiks 4000	316L original
Kinetiks_1	Kinetiks 4000	316L 1st recovery
Kinetiks_2	Kinetiks 4000	316L 2nd recovery
Kinetiks_3	Kinetiks 4000	75wt.% 316L 2nd recovery + 25wt.% 316L original

Fig. 1 Powder collecting system

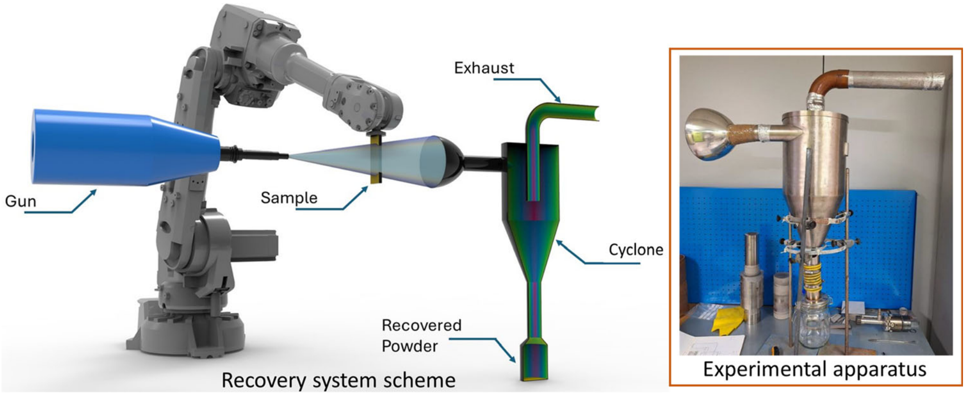

Table 2 316L feedstock powder nominal composition. wt.%

Cr	Ni	Mo	Si	Mg	S	P	Fe
15.9	12.3	2.6	< 2.0	< 0.1	< 0.5	< 0.5	Bal.

constant of 0.94 for cubic crystals, λ is the wavelength, β is the full-width half-maximum (FWHM) at the peak, and 2θ is the peak of interest.

$$\tau = \frac{K \cdot \lambda}{\beta \cdot \cos\theta} \quad \text{(Eq 2)}$$

The powder flow rate and apparent density were assessed using a Hall funnel, following the ASTM B213-03 and ASTM B212-99 standards, respectively. The 316L original nominal composition was obtained by inductively couple plasma (ICP) using a PerkinElmer Optima ICP-OES 3200 RL (Waltham, MA, USA) equipment and is listed in Table 2. The powders were mounted, polished and their microhardness was measured in a Shimadzu HMV (Tokyo, Japan) microhardness tester, applying a load of 0.01 kgf ($HV_{0.01}$) for 15 s. The results are mean values of ten indents.

Table 3 CS deposition parameters

Parameter	PCS100	Kinetiks
N_2 pressure (bar)	60	40
N_2 temperature (°C)	1000	800
Powder feeding (g s^{-1})	0.44	0.41
Standoff distance (mm)	25	25
Robot speed (mm s^{-1})	500	500
Step (mm)	1	1

CS Deposition

CS coatings were deposited on low-carbon steel substrates ($20 \times 50 \times 5$ mm^3) using two different high-pressure CS system: a Plasma Giken PCS100 (Saitama, Japan) and a CGT Kinetiks 4000 (Haun, Germany), simply called Kinetiks, hence forth. Prior to the deposition process, the substrates were sand-blasted with alumina (F24) to a roughness Ra $\approx$ 7 µm measured in a Mitutoyo SJ-210 (Tokyo, Japan). The CS deposition parameters are presented in Table 3. These parameters were previously optimized by the Center of Thermal Spray (CPT) at Universitat de Barcelona research group to achieve the maximum DE. The deposition strategy was the traditional one, a zig-zag-like or raster path with the spray angle perpendicular to the substrate, as presented in detail by Vaz et al. (4). During the deposition with Kinetiks, the system was monitored to collect electrical and gas consumption data. For the energy consumption, an ammeter clamp PCE PCM1 (Tobarra (Albacete), Spain) was used, and the working gas flow was obtained from the CS system data logger.

For a deposition costs evaluation, (3) was used, where C_{CS} is the total cost for the manufacturing in euros (€), PF is the powder feeding rate in g s^{-1}, DE is the deposition efficiency in %, C_{powder} is the powder cost in €·g^{-1}, Q is the gas flow rate in m^3 s^{-1}, C_{gas} is the gas cost in €·m^{-3}, E is the energy consumption in kW, C_{energy} is the energy cost in €·$(kW\ s)^{-1}$, and t is the spraying time in s. The costs assumed for use in (3) were based on mean values in Spain in 2024: 70.00€ for each 10 m^3 N_2 cylinder refilling at 200 bar; energy at 0.43€·$(kW\ h)^{-1}$; and 21.78€·kg^{-1} for 316L irregular powder.

$$C_{CS} = \left[\left(\mathrm{PF} \times \mathrm{DE} \times C_{\mathrm{powder}}\right) + \left(Q \times C_{\mathrm{gas}}\right) + \left(E \times C_{\mathrm{energy}}\right)\right] \times t \qquad \text{(Eq 3)}$$

Sample Characterization

The CS 316L coating cross sections were prepared following the ASTM E1920-03 standard. ImageJ v.1.52a software was used to evaluate the porosity of the coatings, following test method B described in ASTM E2109-14 standard. The porosity calculation was performed by establishing a greyscale threshold on the microstructural images obtained by optical microscopy (OM) with a Leica DMI 5000 (Wetzlar, Germany) microscope. For each coating, six porosity measurements were taken. In addition, a Shimadzu HMV (Tokyo, Japan) microhardness tester was used to perform ten Vickers indents, applying a load of 0.3 kgf ($HV_{0.3}$) for 15 s. The DE was determined by the coating to feedstock powder-sprayed mass ratio.

Results and Discussion

The custom-built cyclone powder recovery system collected the CS-ed unbonded 316L particles through the principle of inertial impaction, generated by centrifugal force. This device is characterized by a settling chamber where gravitational acceleration is replaced by centrifugal acceleration as the particles travel down the cyclone cone. The careful design of the cyclone's conical section induces a change of direction in the lower section of the vortex, while the upward section has a larger radius, resulting in higher tangential velocities. This conical design favors the maximum capture of particles, especially smaller ones, by this gradual reduction in turning radius. This system does not affect the CS deposition process since it does not have influence on the particle velocity or the substrate conditions (e.g., temperature, cleanness, or roughness).

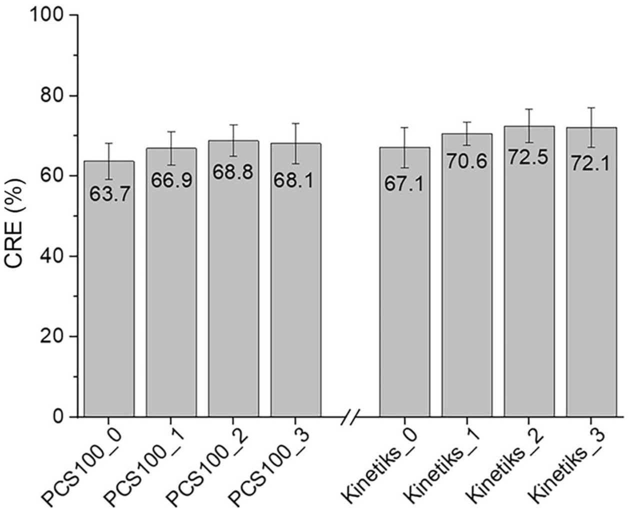

Fig. 2 Cyclone recovery efficiency for 316L original and recovered powders

The CRE results are presented in Fig. 2. Evaluating the average value, the highest CRE was obtained for PCS100_2 and Kinetiks_2, reaching values close to 70%, and the lowest CRE was seen for the CS 316L original, 63.7% for PCS100_0, and 67.1% for Kinetiks_0. Blending the 2nd recovery powder with 25wt.% 316L original slightly reduced the CRE from the pure CS 2nd recovery powders for both CS systems. Considering the standard deviation and the range of CRE values measured, no evolution of CRE could be drawn because statistically, the CRE for all the experiments was found in the same range of values, as seen graphically in Figure 2. Based on these results, it is noticed that the recovery system developed at CPT has the same performance for both CS systems (PCS100 and Kinetiks), even knowing that these systems have different designs, nozzles dimensions, and probably unequal particle jet dispersion.

As interpreted from the apparatus scheme in Fig. 1, the recovery system was placed behind the sample during the deposition and the robot moved the sample performing the raster path to deposit the coating. (1) Also shows that CRE was calculated considering the variable $P_{coating}$., meaning that the recovery system operated, while the deposition was performed. It results in a recovery of particles that did not touch the substrate and particles that impacted on the substrate sides and were slightly deformed. Besides that, some particles rebounded after impacting onto the substrate, and others had their trajectory change to outrange zone of the recovery system, and both were not collected

Fig. 3 SEM images of 316L original and recovered powders

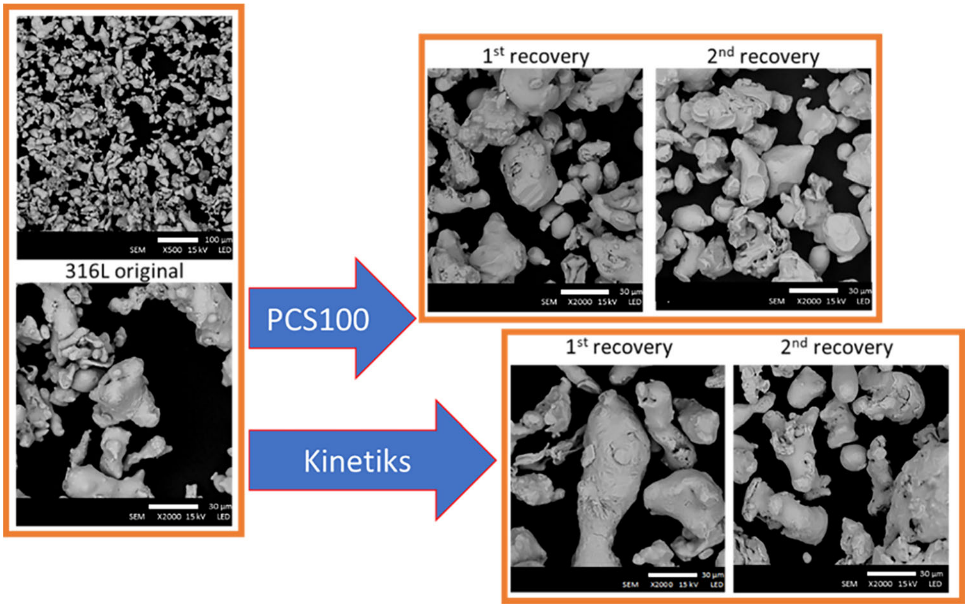

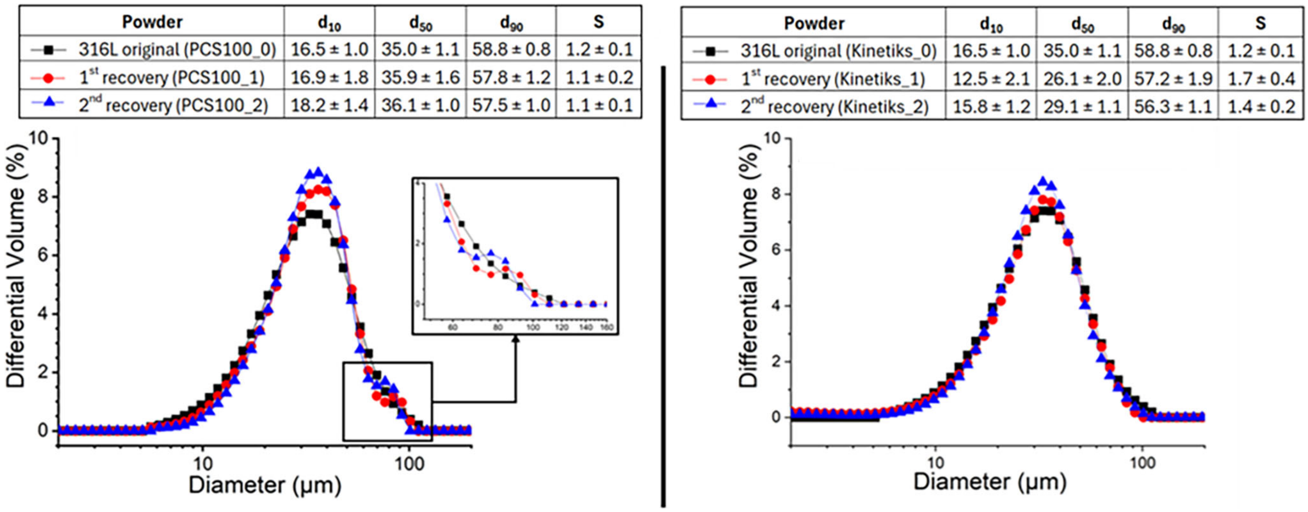

Powder	d_{10}	d_{50}	d_{90}	S
■ 316L original (PCS100_0)	16.5 ± 1.0	35.0 ± 1.1	58.8 ± 0.8	1.2 ± 0.1
● 1st recovery (PCS100_1)	16.9 ± 1.8	35.9 ± 1.6	57.8 ± 1.2	1.1 ± 0.2
▲ 2nd recovery (PCS100_2)	18.2 ± 1.4	36.1 ± 1.0	57.5 ± 1.0	1.1 ± 0.1

Powder	d_{10}	d_{50}	d_{90}	S
■ 316L original (Kinetiks_0)	16.5 ± 1.0	35.0 ± 1.1	58.8 ± 0.8	1.2 ± 0.1
● 1st recovery (Kinetiks_1)	12.5 ± 2.1	26.1 ± 2.0	57.2 ± 1.9	1.7 ± 0.4
▲ 2nd recovery (Kinetiks_2)	15.8 ± 1.2	29.1 ± 1.1	56.3 ± 1.1	1.4 ± 0.2

Fig. 4 Particle size distribution of 316L original and recovered powders

by the recovery system. It helps to understand the CRE below 75% in all the experiments.

Powder Characterization

Figure 3 presents SEM images of the feedstock powders used in this study. The 316L original powder showed an irregular morphology, which is typical of water-atomized powders, due to the rapid cooling and solidification process in this technique. Inert gas-atomized metallic powders, by contrast, present a spherical shape resulting from the more controlled and uniform cooling environment of the gas stream. Besides this, smaller satellite particles were observed bonded to the large particles. Figure 3 shows SEM images of the 1st and 2nd recovery powders. It is noticeable that there is some deformation and change in the particle shape induced by the impact of the unrounded particles to each other, onto the substrate, and onto cyclone walls during the CS deposition.

Figure 4 shows the particle size distribution of the 316L original and recovered powders sprayed with the PCS100 and Kinetiks systems. The percentiles reveal that for PCS100, the d_{50} particle size increased with each recycling cycle from an original d_{50} of 35.0 ± 1.1 to 35.9 ± 1.6 μm in the 1st recovery and to 36.1 ± 1.0 μm in the 2nd recovery; d_{10} also increased from 16.5 ± 1.0 to 16.9 ± 1.8 and 18.2 ± 1.4 μm for the 316L original, to 1st and 2nd recovery, respectively. In the cyclone recovery process, the recovered powder of the cyclone particles at high temperatures and kinetic energy interacts with the cooler and less turbulent environment thermal agglomeration likely occurs due to heat absorption, collisions, and gradual cooling.

Figure 4 also reveals that the curve undergoes an alteration in the 1st and 2nd recovery PCS100 sprayed powders, specifically in the lower right region, approximately around the d_{90} particle diameter. This phenomenon indicates a slight increase in coarse particle size or the formation of agglomerates during the recovery process in the cyclone. For the Kinetiks system, the 1st recovery decreased the d_{10} value from 16.5 ± 1.0 to 12.5 ± 2.1 µm and the d_{50} from 35.0 ± 1.1 to 26.1 ± 2.0 µm, indicating a higher content of fine or fragmented particles that fractured at their impact onto the cyclone walls. The 2nd recovery restored the d_{10} to a size close to the 316L original probably due to an agglomeration of the fine particles or the exhaustion of the finest ones by the exhausting system connected at the top of the recovery system (Figure 1).

It is important to evaluate the span of the particle size distribution because it has been a parameter to classify or predict the powder flowability, as reported by Jenike (Ref 17). The span (S) is given by (4), where d_{10}, d_{50}, and d_{90} are the 10th, 50th, and 90th percentiles of the particle size distribution, respectively. Powders with $S < 1.5$ show good flow properties, while powders with $S > 1.5$ result in rather worse flow properties (Ref 18). For 316L original powder, $S = 1.2 \pm 0.1$, and for the recovered powders this value did not vary much, except for 1st recovery of Kinetiks, which showed $S = 1.7 \pm 0.4$. This could result in worse flowability for this last powder and a good flow rate for the other powders. However, it was not observed for 316L original, which did not flow in the Hall funnel testing, resulting in an unmeasurable flow rate plotted as 0 g s^{-1} in Fig. 5; this is likely because other powder characteristics supplanted it, such as the particle surface roughness, which reduced after flowing through the nozzle and impacting each to other in flight and against the cyclone walls at the recovery step.

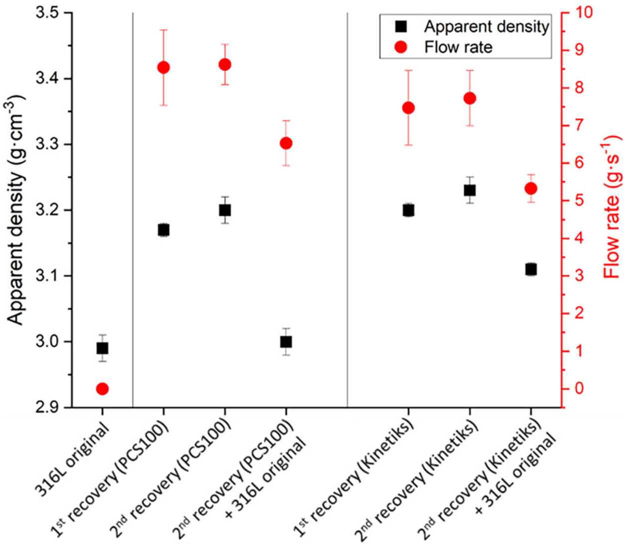

Fig. 5 Apparent density and flowability of 316L original and recovered powders. For the powders blending 75wt.% 2nd recovery + 25wt.% 316L original

$$S = \frac{d_{90} - d_{10}}{d_{50}}; S_{\text{limit}} = 1.5 \quad \text{(Eq 4)}$$

By recovering the powder, its flow rate increased to 8.5 ± 1.0 and 8.6 ± 0.5 g s^{-1} for PCS100_1 and PCS100_2, respectively, and 7.5 ± 1.0 and 7.7 ± 0.7 g s^{-1} for Kinetiks_1 and Kinetiks_2, respectively. However, blending the 2nd recovery powder with 25wt.% 316L original, the flow rate decreased to 6.5 ± 0.6 and 5.3 ± 0.4 g s^{-1} for PCS100 and Kinetiks, respectively. The apparent density of 316L powders also changed by the recovery. The 316L original had 2.99 ± 0.02 g cm^{-3}, while the recovery powders resulted in values around 3.20 g cm^{-3}. However, blending the 2nd recovery powder with 25wt.% 316L original affected the apparent density, returning to the initial value of 3.00 ± 0.02 g cm^{-3} for PCS100 and to 3.11 ± 0.01 g cm^{-3} for Kinetiks.

This helped to improve the apparent density also (e.g., close to 3.20 g cm^{3} against 3.00 g cm^{3} of the 316L original for the PCS100 and Kinetiks systems in Fig. 5), which can be attributed to the particle's surface characteristics and arrangement, following the model proposed by Ben Ohoud et al. (19). Considering the PCS100 and Kinetiks powder feeder systems, a higher flowability and apparent density should benefit spraying feeding because it prevents accumulation of powder (i.e., mountains on certain regions of the feeder, filling properly the small disk holes of the feeder systems). It is important to note that the CS feeders studied in this work do not have a vibratory apparatus that could help for better feeding of low flowability powders, as occurs for other systems (e.g., Metco 9MP series thermal spray powder feeders). Furthermore, although the 316L original did not flow in the Hall funnel testing, the CS feeding rate was good enough for the 316L coating depositions studied in this work.

It is noteworthy that the 2nd recovery powder characteristics were severely influenced by the addition of a small fraction (25 wt.%) of 316L original, which reduced the apparent density, flowability, and the recovery system efficiency CRE. However, it improved the CS-ed 316L coatings properties, as discussed further in this study.

In the comparative analysis of the 316L original and recovered powders XRD diffractograms (Fig. 6), a broadening at the base of the peaks is observed with the recovering process. As the number of recovery cycles increased,

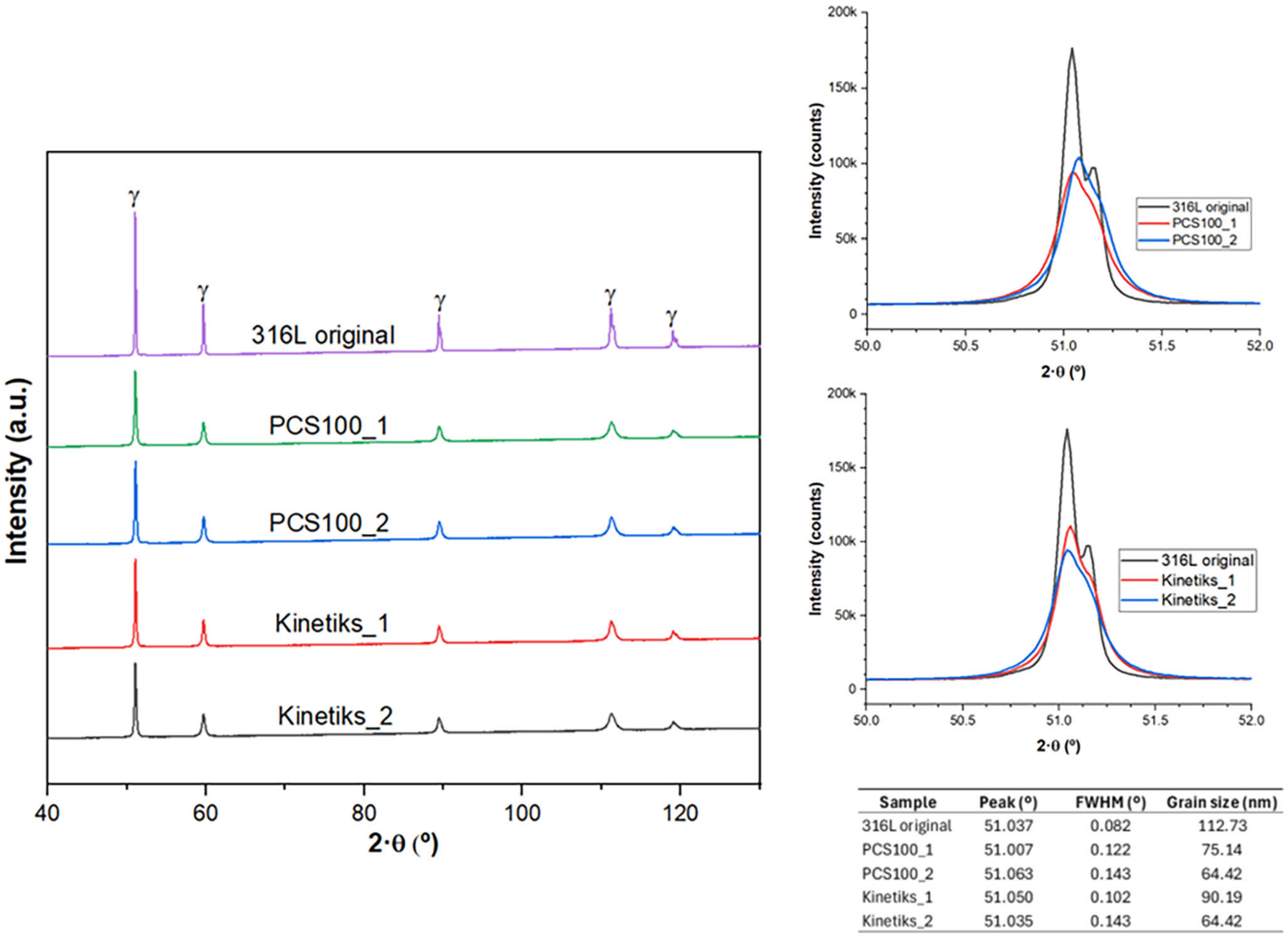

Sample	Peak (°)	FWHM (°)	Grain size (nm)
316L original	51.037	0.082	112.73
PCS100_1	51.007	0.122	75.14
PCS100_2	51.063	0.143	64.42
Kinetiks_1	51.050	0.102	90.19
Kinetiks_2	51.035	0.143	64.42

Fig. 6 Diffractograms of 316L original and recovered powders

there was a noticeable widening of the peak base. This phenomenon can be attributed to: (i) a variation in the average size of crystals; ii) the presence of internal stresses in the crystal structure; (iii) changes in grain orientation; or iv) the existence of impurities and that affect the peak profile (Ref 15).

Regarding the crystallite or mean grain sizes, it was selected the peak at $2\theta = 51.05°$, measured the FWHM, and calculated using (2) the τ values seen in Figure 6, showing a slight reduction of the grain sizes from 112.73 nm for 316L original to 75.14 and 90.19 nm for PCS100_1 and Kinetiks_1, respectively. For PCS100_2 and Kinetiks_2, the crystallite size was 64.42 nm, which is smaller than for the 1st recovery. It can be attributed to dynamic recrystallization during the deposition. For the internal stresses, the literature presents that displacing the peak from its original position can be attributed to a uniform stress distribution, while a peak broadening indicates a nonuniform stress distribution (Ref 20), and the slightly broader peaks seen for recovered powder signs to this last one stress distribution. Grain orientation cannot be affected by CS because the process does not occur in a preferential direction, deforming the particles randomly. The results of phase identification indicate negligible variation between the 316L original and recovered powders. All diffractograms exhibit the same characteristic peaks of γ austenite. No anomalous peaks were detected in any of the samples, suggesting that there is no significant contamination due to reuse of the powders (Ref 16). XRD shows a decrease in the intensity of the γ peaks, as well as a broadening of these peaks, which is associated with an increase in microstrain in the γ phase lattice structure. In general, two deformation mechanisms—dislocation sliding, and ε or α' martensite formation—may occur during plastic deformation of 316L (Ref 21). However, these effects were not seen in CS deposition due to the high strain rate at the impact of the particles since CS experiences strain rate of powder particles in the range of 10^7 to 10^9 s^{-1} at the impact onto the substrate (Ref 22), impeding the α' martensite formation because it is higher than a limit value of 10^5 s^{-1} presented by Chen et al. (23). A lower strain rate can occur in some small volumes of the particles

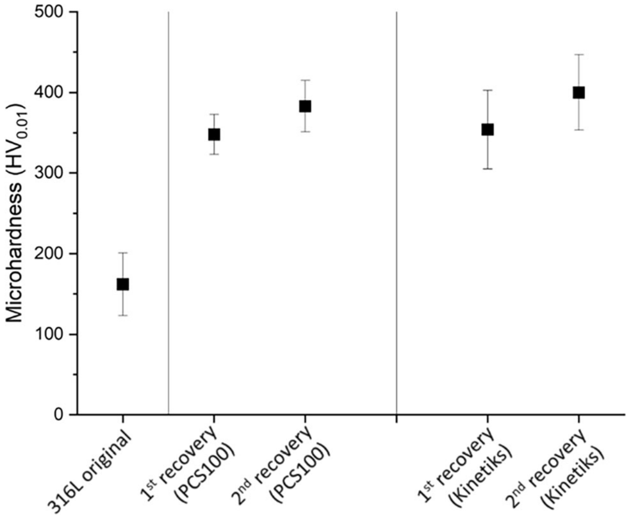

Fig. 7 Microhardness of 316L original and recovered powders

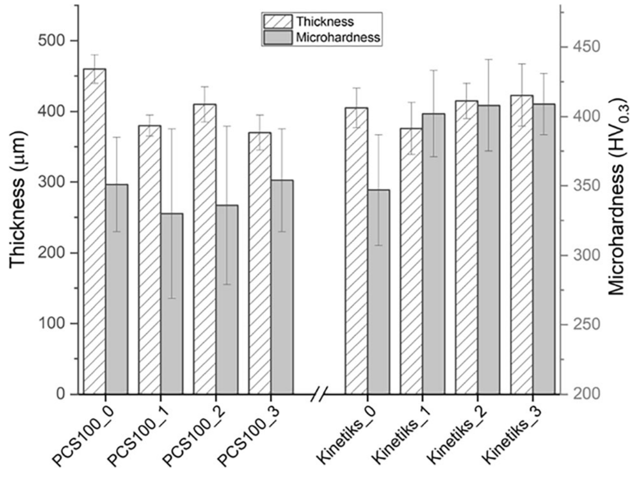

Fig. 9 Thickness and microhardness of CS-ed coatings obtained with 316L original and recovered powders

and martensite can be formed, but another characterization technique should be used to identify this small phase content in the material instead of XRD (e.g., transmission electron microscopy).

During the CS deposition process and subsequent powder recovery, a notable increase in the hardness of the recycled powders was recorded. For the PCS100 system, the hardness escalated from 162 ± 39 $HV_{0.01}$ of the 316L original powder to 348 ± 25 and 383 ± 32 $HV_{0.01}$ of the 1st and 2nd recovery, respectively. Furthermore, with the Kinetiks, the hardness levels were observed at 354 ± 49 $HV_{0.01}$ in the 1st recovery and rose to 400 ± 47 $HV_{0.01}$ in the 2nd one. The increase in hardness after recovery can be attributed to the high temperature during the deposition with the gas at 1000 °C in the gun heating chamber, followed by rapid cooling after spraying, which may have induced changes in the microstructure of the powders. The velocity at which particles are sprayed also plays a crucial role, influencing deformation and impact energy in the cyclone. The plastic deformation of the particles manifests itself in the creation of dislocations in the material's microstructure. These crystalline defects result from plastic deformation and can have a significant impact on the mechanical properties of the material, such as strength and toughness (Ref 24).

Coating Characterization

Figure 8 presents cross sections of CS-ed coatings for the eight sprays. Similar microstructures were produced for all the feedstock powders. The microstructures of the coatings were composed of deformed particles or splats, pores or voids, and inter-particle borders or interfaces—a typical CS microstructure. No oxide layers can be observed, as seen in

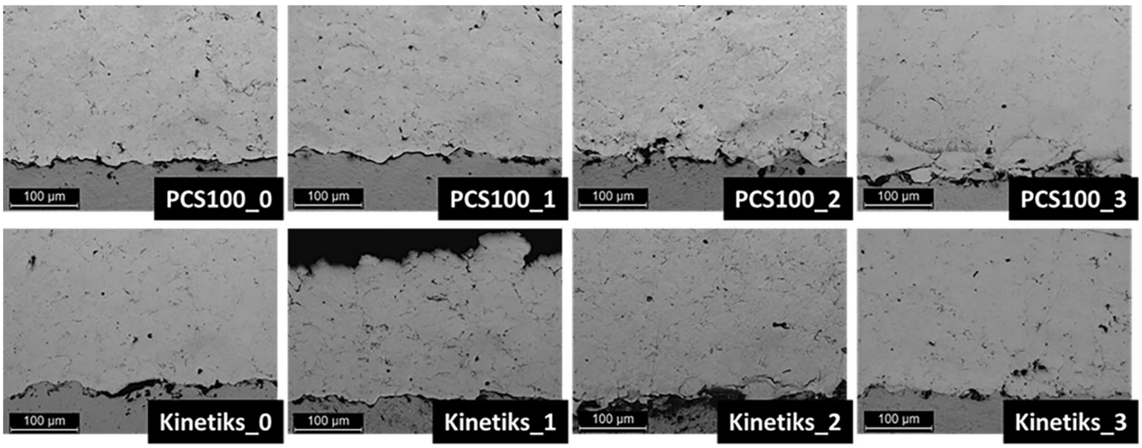

Fig. 8 Microstructure of CS-ed coatings obtained with 316L original and recovered powders

other heat-based thermal spray processes, such as air plasma spray or high-velocity oxy-fuel. The similarity between the microstructures shows that the CS parameters previously optimized by CPT's team for 316L original powder were adequate to obtain a good coating of either 316L original or recovered powders. No higher velocity was needed for obtaining a dense coating for recovered powders, although these powders have higher hardness than 316L original, as seen in Fig. 7.

Figure 9 presents the microhardness and thickness of the CS-ed coatings obtained with 316L original and recovered powders. For the 316L original, PCS100 and Kinetiks produced coatings with an average microhardness of around 350 $HV_{0.3}$, which is close to the microhardness of recovered powders presented in Fig. 7, but higher than the 316L original powder, which was 162 ± 39 $HV_{0.01}$. This indicates that the 316L original particles were submitted to cold working during the CS process. This improves the density of discontinuities, resulting in a higher microhardness, since while phase transformation and hardness increasing can happen by deformation or pseudo-elasticity for low-stack fault energy materials (e.g., shape memory alloys and Fe-Mn alloys (Ref 21, 25)), no phase transformation was observed in the recovered powders, seen in Fig. 6.

For the PCS100 system, the CS coatings obtained with recovered powders appear to result in a lower mean hardness than the 316L original powder coating; however, considering the standard deviations, the values are comparable, which means that no significant hardening was produced by CS a recovered powder. It is likely that either their initial microstructure was maintained or dynamic recrystallization occurred in some volumes of the deposit (Ref 26), reducing the microhardness at those points and impacting on the microhardness mean value. For the Kinetiks CS deposits, the deposition of the 1st recovered powder improved the hardness to values higher than 400 $HV_{0.3}$, which was maintained for depositing the 2nd recovered powder. This indicates that the Kinetiks system imposed a higher deformation of particles at the impact than the PCS100 system, resulting in a higher density of discontinuities and maintenance of fine grains in the material.

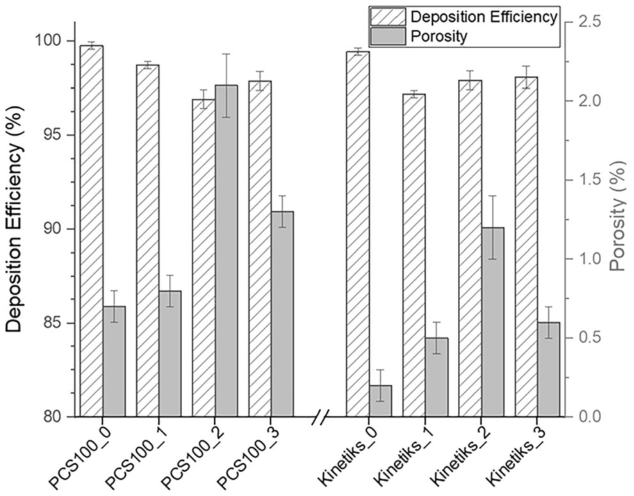

Fig. 10 DE and porosity of CS-ed coatings obtained with 316L original and recovered powders

Figure 9 also presents the thickness obtained for each powder, 316L. A sprayed coating's thickness is a consequence of the DE, particle size, and microstructure, especially the oxide and porosity content and distribution. CS does not produce oxides, which can be observed by the diffractograms of Fig. 6 which do not show oxide peaks for any CS-ed coating. But the porosity presented in Fig. 10 shows that the CS with 2nd recovery powder (PCS100_2 and Kinetiks_2) had a lower deformability than the previous sprayed powders. It resulted in the highest porosity among the samples evaluated: 2.1 ± 0.2% for PCS100 and 1.2 0.2% for Kinetiks. Besides that, the CS 2nd recovery powder had a lower DE than CS 316L original powder, 96.9 ± 0.5 and 97.9 ± 0.6% for PCS100_2 and Kinetiks_2, respectively.

Although the CS 316L DE was high, it is not a fact for many materials or deposition strategies, e.g., CS Inconel or Ti6Al4V and off-normal angles CS strategies (Ref 3). The use of the recovery system can be useful for a deposition on complex geometries instead of a deposition on a simple plate, e.g., depositing a coating on a multi-holed or perforated plate, knowing that most of the sprayed powder will pass through the substrate. In this case, the DE will be high for the particles that reach the substrate (high bonding); however, the global DE can be very low, depending on the substrate geometry, because of the high volume of particles that will pass through the substrate by the holes. These unbonded particles can be recovered and CS-ed again. Besides that, the recovery system keeps collecting the particles during the CS system warm-up time, when the working gas pressure and temperature increase gradually until the setpoint and the powder feeding rate are stabilized before the CS deposition. It is important to consider that this powder wasted during the CS warm-up is not computed in DE determination because, for this calculation, the chronometer starts with the CS deposition, neglecting the warm-up powder waste.

Yeom et al. (27) show that a higher plastic deformation can be achieved by increasing the particle velocity using He as CS working gas, reaching 844 m s^{-1} by mixing 75 vol.% He + 25vol.% N_2, while 635 m s^{-1} was the velocity of particle for pure N_2. However, this is an expensive solution because He is much more costly than N_2. The alternative proposed in this work to overcome this reduction in the coating quality was blending 75wt.% 316L 2nd recovery + 25wt.% 316L original, which resulted in an acceptable porosity level of 1.3% for PCS100_3 and 0.6% for Kinetiks_3, keeping the DE above 98%. It shows that adding a few amounts of 316L original to the hard 2nd recovery powder restores the material deformability and plasticity, compensating for the lower plasticity seen after two reuses.

Study of Costs

For evaluating the effect of recovering and reusing powders for CSAM, in an idealized 50 × 50 × 50 mm^3 316L deposit was considered for the analysis and one only system—the Kinetiks system was used—since the powder reuse efficiency was the same for both systems. The analysis was performed for Kinetiks system. The CSAM traditional strategy—raster pattern—used makes a pyramid-like shape for tall deposits, as presented in detail by Vaz et al. (4); however, this effect was neglected for this analysis, and a perfect cube shape was idealized lists the parameters for the economic analysis, considering the 316L original and recovered powders, and the previously evaluated properties of the coatings, such as porosity, DE, and thickness per layer. The time computed ignores the CS spraying off the substrate (e.g., robot trajectory changes and inter-layer time).

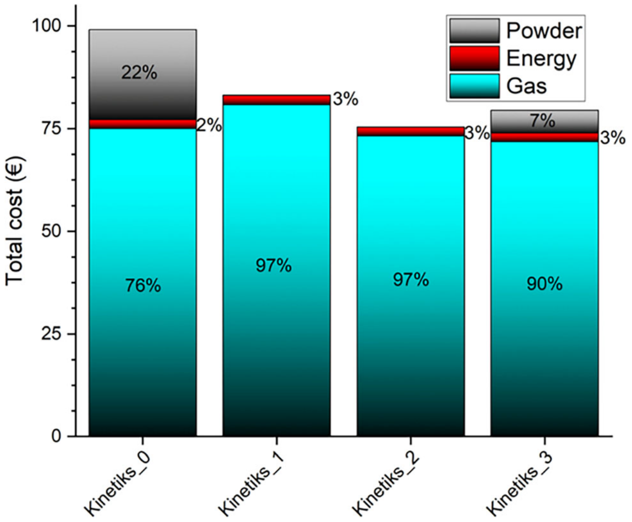

Fig. 11 Total costs to build a 50 × 50 × 50 mm^3 316L by CS with 316L original and recovered powders

Considering commercial prices for gas, energy, and powder acquisition, but neglecting the human resources in Spain, the total costs for building the 316L cube are presented in Fig. 11. It is noticed that the energy consumption is the lowest value, which is almost constant for all the depositions, between 2.09€ and 2.35€. The gas costs (N_2) slightly varied with the spraying time presented in Table 4, varying 71.87€ for Kinetiks_3 to 80.85€ for Kinetiks_2. However, the highlight is the powder costs, which was 21.86€ for Kinetiks_0 (which sprayed 316L original powder) and costless for Kinetiks_1 and Kinetiks_2 (which sprayed the wasted powder from the previous depositions). A small cost was associated with Kinetiks_3, due to the use of 25 wt.% of original powder blended with the reused one.

The effect of powder consumption on the final costs of a CS coating or a CSAM-ed deposit is strongly associated with the cost of the powder itself. The literature has presented that CS has the ability to spray an irregular powder or a spherical powder, achieving the same coating properties, as studied by Vaz et al. (9) for CS 316L and McDonald et al. (11) for CS Ti. Vargas-Uscategui et al. (28) employed irregular shape hydride–dehydride (HDH) and spherical (Ref 29) pure Ti for CSAM, obtaining similar microstructures, especially a low porosity for expensive and less costly feedstock powders. Regarding the powder production costs and, consequently, their selling prices, Boisvert et al. (30) showed that water-atomized powders are 3–9 times cheaper than gas-atomized ones, supporting the case for research and development in the use of irregular powders for CS.

Figure 11 shows that most CS costs are associated with N_2 consumption, which could be even higher by using He as working gas. However, the literature has presented that although this expensive gas accelerates the particle up to higher velocities, the quality of CS-ed coating can be the same by setting adequate CS parameters for N_2, employing CS hybrid systems, or performing post-treatment (Ref 31, 32). For CS, the working gas is accelerated by flowing through a convergent-divergent nozzle after being heated by electric resistance in a chamber, consuming energy. However, this energy consumption represented only 3% of the CS deposition costs, and research efforts on reducing the energy consumption appear to not significantly affect the CS deposition global costs.

Table 4 CSAM 316L cube data for economic analysis.

	Kinetiks_0	Kinetiks_1	Kinetiks_2	Kinetiks_3
Number of layers	124	132	121	119
Powder fed (g)	1003	959	1018	1015
CSAM time (s)	620	660	605	595

In the present study, the powder acquisition resulted in a considerable contribution to the CS global costs: 22% by depositing 316L original. This supports research alternatives to reduce the feedstock powders costs, especially for CS thick coatings, large areas, or large CSAM deposits. This work already employed a low-cost 316L powder; however, if a spherical 316L feedstock powder were selected, the costs would be at least 5 times higher, and instead of 22% the quote for the powder in the CS global costs would be 56%, surpassing the gas costs. In other words, recovering this powder can reduce global costs to less than half of the cost of using original or new powder. This is a factor to be considered, especially for expensive powders or powders that are still not found in a less expensive option, such as Ti6Al4V or HEAs.

Conclusions

In this study, 316L coatings were deposited using two high-pressure CS systems, and the unbonded particles were recovered and sprayed again. After subsequently characterizing the coatings, the following conclusions can be drawn:

1. The cyclone powder recovery system developed at the CPT (Fig. 1) has proven effective in capturing between 63 and 73% of the unbonded powder during CS depositions without any deleterious effect on the CS deposition process. This collection system has made it possible to recover a significant percentage of the powders that was previously considered waste, which represents an important advance in the optimization of resources and the reduction of waste in the process;
2. The recovered powders have a significant increase in hardness (Fig. 7), as the CS-ed particle travels at high temperature and pressure, impacting onto the substrate and hitting the cyclone walls. The plastic deformation manifests itself in the creation of dislocations in the microstructure of the material and consequently an increase in the hardness of the powder;
3. The coatings made with 316L original and the 1st recovery powders have similar quality and porosity (Figs. 9 and 10); however, depositing the 2nd recovery powder, the porosity increases with both CS systems, showing a reduction of powder plasticity by increasing the recovery cycles;
4. Using a blend 75wt.% 2nd recovery + 25wt.% original powder restores the CS coating quality to similar porosity as seen for pure 316L original coating (Fig. 10), indicating that the plasticity of the 25wt.% original supplants the stiffness of the 75wt.% 2nd recovery one;
5. The reuse of powders stands out as a strategy that not only favors environmental sustainability, but also presents substantial economic advantages, which can reach half of the CS deposition global costs (Fig. 11), increasing the profitability and efficiency of these processes.

Acknowledgments The author thanks the "Knowledge Generation Projects 2021" program from the Ministry of Science and Innovation (Spain), grant number PID 2021-128917NA-I00, financed by MICIU/AEI/https://doi.org/10.13039/501100011033 and for FEDER, UE. E.R. Ramírez and E.T. Diaz are Ph.D. students' fellows of COLCIENCIAS—Ministry of Science, Technology, and Innovation of Colombia, call for PhD applications 885-2020 and 906-2021.

Funding Open Access funding provided thanks to the CRUE-CSIC agreement with Springer Nature.

References

1. M.R. Rokni, S.R. Nutt, C.A. Widener, V.K. Champagne and R.H. Hrabe, Review of Relationship Between Particle Deformation, Coating Microstructure, and Properties in High-Pressure Cold Spray, *J. Therm. Spray Technol.*, 2017, **26**, p 1308-1355. https://doi.org/10.1007/s11666-017-0575-0
2. H. Assadi, F. Gärtner, T. Stoltenhoff and H. Kreye, Bonding Mechanism in Cold Gas Spraying, *Acta Mater.*, 2003, **51**, p 4379-4394. https://doi.org/10.1016/S1359-6454(03)00274-X
3. R.F. Vaz, A. Garfias, V. Albaladejo, J. Sanchez and I.G. Cano, A Review of Advances in Cold Spray Additive Manufacturing, *Coatings*, 2023 https://doi.org/10.3390/coatings13020267
4. R.F. Vaz, V. Albaladejo-Fuentes, J. Sanchez, U. Ocaña, Z.G.Z.G. Corral, H. Canales and I.G. Cano, Metal Knitting: A New Strategy for Cold Gas Spray, *Materials (Basel).*, 2022, **15**, p 1-17. https://doi.org/10.3390/ma15196785
5. L.H. Guilherme, A.V. Benedetti, C.S. Fugivara, R. Magnabosco and M.F. Oliveira, Effect of MAG Welding Transfer Mode on Sigma Phase Precipitation and Corrosion Performance of 316L Stainless Steel Multi-pass Welds, *J. Mater. Res. Technol.*, 2020, **9**, p 10537-10549. https://doi.org/10.1016/j.jmrt.2020.07.039

6. E.R.I. Mahmoud, S.Z. Khan and M. Ejaz, Laser Surface Cladding of Mild Steel with 316L Stainless Steel for Anti-corrosion Applications, *Mater. Today Proc.*, 2021, **39**, p 1029-1033. https://doi.org/10.1016/j.matpr.2020.04.763
7. M. Hassani-gangaraj, D. Veysset, V.K. Champagne, K.A. Nelson and C.A. Schuh, Adiabatic Shear Instability is Not Necessary for Adhesion in Cold Spray, *Acta Mater.*, 2018, **158**, p 430-439. https://doi.org/10.1016/j.actamat.2018.07.065
8. A. Haider and O. Levenspiel, Drag Coefficient and Terminal Velocity of Spherical and Nonspherical Particles, *Powder Technol.*, 1989, **58**, p 63-70. https://doi.org/10.1016/0032-5910(89)80008-7
9. R.F. Vaz, A. Silvello, J. Sanchez, V. Albaladejo and I. García-Cano, The Influence of the Powder Characteristics on 316l Stainless Steel Coatings Sprayed by Cold Gas Spray, *Coatings*, 2021, **11**, p 1-18. https://doi.org/10.3390/coatings11020168
10. V.S. Bhattiprolu, K.W. Johnson, O.C. Ozdemir and G.A. Crawford, Influence of Feedstock Powder and Cold Spray Processing Parameters on Microstructure and Mechanical Properties of Ti-6Al-4V Cold Spray Depositions, *Surf. Coatings Technol.*, 2018, **335**, p 1-12. https://doi.org/10.1016/j.surfcoat.2017.12.014
11. D. MacDonald, R. Fernández, F. Delloro and B. Jodoin, Cold Spraying of Armstrong Process Titanium Powder for Additive Manufacturing, *J. Therm. Spray Technol.*, 2017, **26**, p 598-609. https://doi.org/10.1007/s11666-016-0489-2
12. M. Jeandin, G. Rolland, L.L. Descurninges and M.H. Berger, Which Powders for Cold Spray?, *Surf. Eng.*, 2014, **30**, p 291-298. https://doi.org/10.1179/1743294414Y.0000000253
13. C.-J. Li, H.-T. Wang, Q. Zhang, G.-J. Yang, W.-Y. Li and H.L. Liao, Influence of Spray Materials and Their Surface Oxidation on the Critical Velocity in Cold Spraying, *J. Therm. Spray Technol.*, 2010, **19**, p 95-101. https://doi.org/10.1007/s11666-009-9427-x
14. V. Viswanathan, N.K. Katiyar, G. Goel, A. Matthews and S. Goel, Role of Thermal Spray in Combating Climate Change, *Emergent Mater.*, 2021, **4**, p 1515-1529. https://doi.org/10.1007/s42247-021-00307-1
15. C. Lu, R. Zhang, M. Xiao, X. Wei, Y. Yin, Y. Qu, H. Li, P. Liu, X. Qiu and T. Guo, A Comprehensive Characterization of Virgin and Recycled 316L Powders During Laser Powder Bed Fusion, *J. Mater. Res. Technol.*, 2022, **18**, p 2292-2309. https://doi.org/10.1016/j.jmrt.2022.03.125
16. K.L. Terrassa, J.C. Haley, B.E. MacDonald and J.M. Schoenung, Reuse of Powder Feedstock for Directed Energy Deposition, *Powder Technol.*, 2018, **338**, p 819-829. https://doi.org/10.1016/j.powtec.2018.07.065
17. A. Jenike, *Storage and flow of solids*, 1964 https://doi.org/10.2172/5240257
18. J. Zegzulka, D. Gelnar, L. Jezerska, R. Prokes and J. Rozbroj, Characterization and Flowability Methods for Metal Powders, *Sci. Rep.*, 2020, **10**, p 21004. https://doi.org/10.1038/s41598-020-77974-3
19. M. Ben Ohoud, F. Obrecht, L. Gatineua, P. Levitz and H. Van Damme, Surface Area, Mass Fractal Dimension, and Apparent Density of Powders, *J. Colloid Interface Sci.*, 1988 https://doi.org/10.1016/0021-9797(88)90336-0
20. R.F. Vaz, A. Garfias, V. Albaladejo, J. Sanchez and I.G. Cano, How Increasing Cold Spray Coatings Thickness Affects Their Residual Stress and Properties, *Surf. Coatings Technol.*, 2024, **485**, 130867. https://doi.org/10.1016/j.surfcoat.2024.130867
21. N. Solomon and I. Solomon, Deformation Induced Martensite in AISI 316 Stainless Steel, *Rev. Metal.*, 2010, **46**, p 121-128. https://doi.org/10.3989/revmetalm.0920
22. K. Spencer and M.-X. Zhang, Optimisation of Stainless Steel Cold Spray Coatings Using Mixed Particle Size Distributions, *Surf. Coat. Technol.*, 2011, **205**, p 5135-5140. https://doi.org/10.1016/j.surfcoat.2011.05.020
23. A.Y. Chen, H.H. Ruan, J. Wang, H.L. Chan, Q. Wang, Q. Li and J. Lu, The Influence of Strain Rate on the Microstructure Transition of 304 Stainless Steel, *Acta Mater.*, 2011, **59**, p 3697-3709. https://doi.org/10.1016/j.actamat.2011.03.005
24. H.-S. Kim and S.-H. Park, Significant Dislocation Strengthening of Stainless Steel 316L Via Co-directed Energy Deposition of Silica, *Mater. Sci. Eng. A*, 2024, **891**, 145948. https://doi.org/10.1016/j.msea.2023.145948
25. R.F. Vaz, L.L. Silveira, J.R. Cruz and A.G.M. Pukasiewicz, Cavitation Resistance of FeMnCrSi Coatings Processed by Different Thermal Spray Processes, *Hybrid Adv.*, 2024, **5**, 100125. https://doi.org/10.1016/j.hybadv.2023.100125
26. Y. Zou, W. Qin, E. Irissou, J. Legoux, S. Yue and J.A. Szpunar, Dynamic Recrystallization in the Particle/Particle Interfacial Region of Cold-Sprayed Nickel Coating: Electron Backscatter Diffraction Characterization, *Scr. Mater.*, 2009, **61**, p 899-902. https://doi.org/10.1016/j.scriptamat.2009.07.020
27. H. Yeom, T. Dabney, N. Pocquette, K. Ross, F.E. Pfefferkorn and K. Sridharan, Cold Spray Deposition of 304L Stainless Steel to Mitigate Chloride-Induced Stress Corrosion Cracking in Canisters for Used Nuclear Fuel Storage, *J. Nucl. Mater.*, 2020, **538**, p 152254. https://doi.org/10.1016/j.jnucmat.2020.152254
28. A. Vargas-Uscategui, P.C. King, S. Yang, C. Chu and J. Li, Toolpath Planning for Cold Spray Additively Manufactured Titanium Walls and Corners: Effect on Geometry and Porosity, *J. Mater. Process. Technol.*, 2021, **298**, 117272. https://doi.org/10.1016/j.jmatprotec.2021.117272
29. A. Vargas-Uscategui, P.C. King, M.J. Styles, M. Saleh, V. Luzin and K. Thorogood, Residual Stresses in Cold Spray Additively Manufactured Hollow Titanium Cylinders, *J. Therm. Spray Technol.*, 2020, **29**, p 1508-1524. https://doi.org/10.1007/s11666-020-01028-3
30. M. Boisvert, D. Christopherson, P. Beaulieu and G. L'Espérance, Treatment of Ferrous Melts for the Improvement of the Sphericity of Water Atomized Powders, *Mater. Des.*, 2017, **116**, p 644-655. https://doi.org/10.1016/j.matdes.2016.12.059
31. A.G.M. Pukasiewicz, W.R. de Oliveira, R.F. Váz, G.B. de Souza, F.C. Serbena, S. Dosta and I.G. Cano, Influence of the Deposition Parameters on the Tribological Behavior of Cold Gas Sprayed FeMnCrSi Alloy Coatings, *Surf. Coat. Technol.*, 2021, **428**, p 127888. https://doi.org/10.1016/j.surfcoat.2021.127888
32. R. Nikbakht, C.V. Cojocaru, M. Aghasibeig, É. Irissou, T.-S. Kim, H.S. Kim and B. Jodoin, Cold Spray and Laser-Assisted Cold Spray of CrMnCoFeNi High Entropy Alloy Using Nitrogen as the Propelling Gas, *J. Therm. Spray Technol.*, 2022, **31**, p 1129-1142. https://doi.org/10.1007/s11666-022-01361-9